*International Journal of Engineering & Applied Sciences (IJEAS)*
*Vol.7, Issue 2(2015)26-44*

# ON THE ONSET OF DEAN VORTICES AND UNSTEADY SOLUTIONS THROUGH A CURVED RECTANGULAR DUCT OF LARGE ASPECT RATIO

*Poly Rani Shaha, Sajal Kanti Rudro, Nayan Kumar Poddar and Rabindra Nath Mondal* [*]

*Department of Mathematics, Jagannath University, Dhaka-1100, Bangladesh*
[*]*E-mail address*: *rnmondal71@yahoo.com*

**Abstract**

*The present study covers a comprehensive numerical study on fully developed two-dimensional flow of viscous incompressible fluid through a curved rectangular duct of aspect ratio 4. Numerical calculations are carried out by using a spectral method, and covering a wide range of the Dean number,* $100 \le Dn \le 1000$, *for two cases of the duct curvature, Case I:* $\delta = 0.001$ *and Case II:* $\delta = 0.1$. *The main concern of the present study is to find out effects of curvature as well as formation of Dean vortices on unsteady solutions as the unsteady flow is steady-state, periodic, multi-periodic or chaotic, if the Dn is increased. Time evolution calculations show that the steady-state flow turns into chaotic flow through various flow instabilities, if Dn is increased no matter what the curvature is. It is found that the unsteady flow is a steady-state solution for small Dn`s, and it oscillates periodically or non-periodically (chaotic) between two-, four-, six-, eight- ten- and twelve-vortex solutions, if Dn is increased. In this study, we obtained multi-vortex solutions due to strong centrifugal force. It is found that the chaotic solution is weak for small Dn's but strong as Dn becomes large. It is also found that the axial flow shifted to the outer wall of the duct as Dn increases.*

**Keywords:** Curved duct; secondary flow; unsteady solutions; Dean number; aspect ratio.

## 1. Introduction

The Fluid flow through curved ducts has been extensively studied for a wide range of applications with a key base of heat transfer and mixing enhancement. Today, the flows in curved non-circular ducts are of increasing importance in micro-fluidics, where lithographic methods typically produce channels of square or rectangular cross-section. These channels are extensively used in many engineering applications, such as in turbo-machinery, refrigeration, air conditioning systems, heat exchangers, rocket engine, internal combustion engines and blade-to-blade passages in modern gas turbines. Changes in cross-sectional shape and curvature of the duct axis are of particular concern because these lead to vortical motions, flow reversals, and unsteadiness. In a curved duct, centrifugal forces are developed in the flow due to channel curvature causing a counter rotating vortex motion applied on the axial flow through the channel. This creates characteristics spiraling fluid flow in the curved passage known as secondary flow. At a certain critical flow condition and beyond, additional pairs of counter rotating vortices appear on the outer concave wall of curved fluid passages which are known as *Dean vortices*, in recognition of the pioneering work in this field by Dean [1]. After that, many theoretical and experimental investigations have been done by keeping this flow in mind; for instance, the articles by Berger et al. [2], Nandakumar and Masliyah [3], and Ito [4] may be referenced.

Numerical solutions should be validated by the experimental results. Therefore, many researchers studied fluid flows in curved ducts using experimental techniques. Flow through a curved rectangular duct has been investigated, both experimentally and numerically, with large aspect ratio by Akiyama et al. [5]. Ligrani and Niver [6] found secondary vortex patterns doing experiments in curved channels for Dean numbers from 40 to 220 and aspect ratio of 1 to 40, in which the photographs illustrated the evidence of a pair of counter-rotating Dean vortices. Yamamoto et al. [7] investigated

secondary flows in a curved duct of square cross section using flow visualization technique. The photographs were taken by changing the Dean number at a constant Taylor number and received a good agreement with their numerical result. Bara et al. [8, 9] studied fully developed incompressible flow in curved square ducts using both experimental and numerical techniques, and obtained two-vortex flow at $Dn$ = 125 and four-vortex at $Dn$ = 137 by Laser Doppler Velocimetry (LDV) measurements. An early analytical and experimental investigations, such as Baylis [10], Humphrey et al. [11], concluded that Dean number was solely responsible for secondary flow and Dean instability in the curved passages. However, later studies with curved rectangular ducts by Cheng et al. [12], Ghia and Sokhey [13] and Sugiyama et al. [14] have shown that the Dean instability is also dependent on the aspect ratio and curvature ratio along with the Dean number. Chandratilleke and Nursubyakto [15] reported a 2-dimensional study to examine the effects of curvature ratio and aspect ratio as well as the wall heat flux. Yanase et al. [16] investigated flow in a curved duct and classified the flow range into three different regimes; steady-stable, periodic and chaotic. They used spectral method to see the field response against perturbation and discovered that while for low flow rate system is confidently stable against perturbation it will turn into periodic and even chaotic behaviors for higher flow rates. Norouzi et al. [17] investigated the inertial and creeping flow of a second-order fluid in a curved duct with square cross-section by using finite difference method. The effect of centrifugal force due to the curvature of the duct and the opposing effects of the first and second normal stress difference on the flow field were investigated in that study. Recently, Chandratilleke et al. [18] presented a numerical investigation to examine the secondary vortex motion and heat transfer process in fluid flow through curved rectangular ducts of aspect ratios 1 to 6. Very recently, an analytical solution for incompressible viscous flow through the curved ducts with rectangular cross-section has been made by Norouzi and Biglari [19] by using perturbation method. The effect of duct curvature and aspect ratio on flow field was investigated in that study.

Time dependent analysis of fully developed curved duct flows was initiated by Yanase and Nishiyama [20] for a rectangular cross section. In that study, they investigated unsteady solutions for the case where dual solutions exist. The time-dependent behavior of the flow in a curved rectangular duct of large aspect ratio was investigated, in detail, by Yanase et al. [21] numerically. They performed time-evolution calculations of the unsteady solutions with and without symmetry condition and showed that periodic oscillations appear with symmetry condition while aperiodic time variation without symmetry condition. Wang and Liu [22] performed numerical as well as experimental investigations of periodic oscillations for the fully developed flow in a curved square duct. Flow visualization in the range of Dean numbers from 50 to 500 was conducted in their experiment. They showed, both experimentally and numerically, that a temporal oscillation takes place between symmetric/asymmetric 2-cell and 4-cell flows when there are no stable steady solutions. Yanase et al. [23] performed numerical investigation of isothermal and non-isothermal flows through a curved rectangular duct and addressed the time-dependent behavior of the unsteady solutions. Recently, Mondal et al. [24, 25] performed numerical prediction of time-dependent solutions for the flow through a curved square duct and discussed the transitional behavior of the unsteady solutions. Very recently, Mondal et al. [26] investigated spectral numerical study for non-isothermal flow through a curved rectangular duct of aspect ratios 1 to 3, and showed that the steady-state flow turns into chaotic flow through various flow instabilities if the aspect ratio is increased. However, transient behavior of the unsteady solutions is not yet resolved for the flow through a curved rectangular duct of large aspect ratio with the effects of curvatures, which motivated the present study to fill up this gap. In the present paper, we investigate unsteady flow characteristics for fully developed two-dimensional flow of viscous incompressible fluid through a curved rectangular duct of aspect ratio 4 with curvatures 0.001 and 0.1. Flow characteristics are studied by using a spectral-based numerical scheme over a wide range of the Dean number.

## 2. Governing Equations

Consider a hydro-dynamically fully developed two-dimensional (2-D) flow of viscous incompressible fluid through a curved rectangular duct with constant curvature. The cross section of the duct is a rectangle with width $2d$ and height $2h$. The $x$, $y$ and $z$ axes are taken to be in the horizontal, vertical, and axial directions, respectively. It is assumed that the flow is uniform in the axial direction (*i.e.* in the z direction), and that it is driven by a constant pressure gradient $G$ along the center-line of the duct, that is, the main flow in the axial direction as shown in Fig. 1.

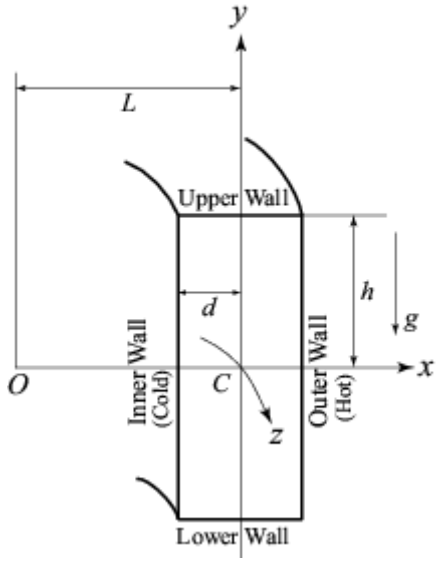


**Figure 1:** Coordinate system of the curved rectangular duct.

The dimensional variables are non-dimensionalized by using the representative length $d$, the representative velocity $U_0 = \frac{\upsilon}{d}$, where $\upsilon$ is the kinematic viscosity of the fluid. We introduce the non-dimensional variables defined as

$$x = \left(\frac{x'}{d} - \frac{1}{\delta}\right),\ y = \frac{y'}{d},\ z = \frac{z'}{d} \quad u = \frac{u'}{U_0},\quad v = \frac{v'}{U_0},\quad w = \frac{\sqrt{2\delta}}{\mathrm{U_o}} w',$$

$$t = \frac{U_0}{d} t',\quad \delta = \frac{d}{L},\quad P = \frac{P'}{\rho U_0^2},$$

where $u, v$ and $w$ are the non-dimensional velocity components in the $x, y$ and $z$ directions, respectively ; $t$ is the non-dimensional time, $P$ is the non-dimensional pressure, $\delta$ is the non-dimensional curvature defined as $\delta = \frac{d}{L}$, Henceforth, all the variables are non-dimensionalized if not specified.

Since the flow field is uniform in the $z$-direction, the sectional stream function $\psi$ is introduced in the $x$- and $y$-directions as follows:

$$u = \frac{1}{1+\delta x}\frac{\partial \psi}{\partial y},\quad v = -\frac{1}{1+\delta x}\frac{\partial \psi}{\partial x} \tag{1}$$

Then basic equations for the axial flow ($w$) and stream function of the secondary flow ($\psi$) are derived from the Navier-Stokes equations with the *Boussinesq approximation* as:

$$(1+\partial x)\frac{\partial w}{\partial t}+\frac{1}{4}\frac{\partial(w,\psi)}{\partial(x,y)}-D_n+\frac{\delta^2}{(1+\delta x)}=(1+\delta x)\Delta_2 w-\frac{1}{4}\frac{\delta}{(1+\delta x)}\frac{\partial\psi}{\partial y}w+\delta\frac{\partial w}{\partial x}, \tag{2}$$

$$\begin{aligned}\left(\Delta_2-\frac{\delta}{1+\delta x}\frac{\partial}{\partial x}\right)\frac{\partial\psi}{\partial t}&=-\frac{1}{4(1+\delta x)}\frac{\partial(\Delta_2\psi,\psi)}{\partial(x,y)}+\frac{\delta}{4(1+\delta x)^2}\\ &\times\left[\frac{\partial\psi}{\partial y}\left(2\Delta_2\psi-\frac{3\delta}{1+\delta x}\frac{\partial\psi}{\partial x}+\frac{\partial^2\psi}{\partial x^2}\right)-\frac{\partial\psi}{\partial x}\frac{\partial^2\psi}{\partial x\partial y}\right]+\frac{\delta}{(1+\delta x)^2}\left[3\delta\frac{\partial^2\psi}{\partial x^2}-\frac{3\delta^2}{1+\delta x}\frac{\partial\psi}{\partial x}\right]\\ &-\frac{2\delta}{(1+\delta x)}\frac{\partial}{\partial x}\Delta_2\psi+\frac{1}{4}w\frac{\partial w}{\partial y}+\Delta_2^2\psi,\end{aligned} \tag{3}$$

Where $$\Delta_2\equiv\frac{\partial^2}{\partial x^2}+\frac{1}{16}\frac{\partial^2}{\partial y^2}, \quad \frac{\partial(f,g)}{\partial(x,y)}\equiv\frac{\partial f}{\partial x}\frac{\partial g}{\partial y}-\frac{\partial f}{\partial y}\frac{\partial g}{\partial x}.$$

The Dean number, *Dn*, which appears in equation (2) is defined

$$Dn=\frac{Gd^3}{\mu v}\sqrt{\frac{2d}{L}}$$

The no-slip boundary conditions for $w$ and $\psi$ are taken as

$$w(\pm1,y)=w(x,\pm1)=\psi(\pm1,y)=\psi(x,\pm1)=\frac{\partial\psi}{\partial x}(\pm1,y)=\frac{\partial\psi}{\partial y}(x,\pm1)=0, \tag{4}$$

In the present study, we calculate unsteady solutions of the flow for the curved rectangular duct of aspect ratio 4 over the Dean number $100\le Dn\le1000$ for cases of the duct curvatures, Case I: Curvature $\delta=0.001$ and Case II: Curvature $\delta=0.1$.

## 3. Numerical Calculations

In order to solve the Eqs. (2) and (3) numerically, the spectral method is used. This is the method which is thought to be the best numerical method to solve the Navier-Stokes equations as well as the energy equation (Gottlieb and Orazag [27]). Details of this method are discussed in Mondal [28]. By this method the variables are expanded in a series of functions consisting of the Chebyshev polynomials. That is, the expansion functions $\Phi_n(x)$ and $\Psi_n(x)$ are defined as

$$\Phi_n(x)=(1-x^2)C_n(x),\ \Psi_n(x)=(1-x^2)^2C_n(x), \tag{5}$$

where $C_n(x)=cos(n\,cos^{-1}(x))$ is the $n$-th order Chebyshev polynomial. $w(x,y,z)$ and $\psi(x,y,t)$ are expanded in terms of $\Phi_n(x)$ and $\Psi_n(x)$ as

$$\left.\begin{aligned} w(x,y,z) &= \sum_{m=0}^{M}\sum_{n=0}^{N} w_{mn}(t)\Phi_m(x)\Phi_n(y), \\ \psi(x,y,t) &= \sum_{m=0}^{M}\sum_{n=0}^{N} \psi_{mn}(t)\Psi_m(x)\Psi_n(y). \end{aligned}\right\} \tag{6}$$

where $M$ and $N$ are the truncation numbers in the $x$- and $y$-directions, respectively. The expansion coefficients $w_{mn}$ and $\psi_{mn}$ are then substituted into the basic Eqs. (2) and (3) and the collocation method is applied. As a result, the nonlinear algebraic equations for $w_{mn}$ and $\psi_{mn}$ are obtained. The collocation points are taken to be

$$\left.\begin{aligned} x_i &= \cos\left[\pi\left(1-\frac{i}{M+2}\right)\right], \qquad i = 1,\ldots,M+1 \\ y_j &= \cos\left[\pi\left(1-\frac{j}{N+2}\right)\right]. \qquad j = 1,\ldots,N+1 \end{aligned}\right\} \tag{7}$$

In the present study, for necessary accuracy of the solutions, we use $M$ = 16 and $N$ = 60. Then, in order to calculate the unsteady solutions, the Crank-Nicolson and Adams-Bashforth methods together with the function expansion (6) and the collocation method are applied to Eqs. (2) and (3)

## 4. Resistance Coefficient

The resistant coefficient $\lambda$ is used as the representative quantity of the flow state. It is also called the *hydraulic resistance coefficient*, and is generally used in fluids engineering, defined as

$$\frac{P_1^* - P_{21}^*}{\Delta_{z^*}} = \frac{\lambda}{d_h^*}\frac{1}{2}\rho\langle\omega^*\rangle^2 \tag{8}$$

where quantities with an asterisk (*) denote dimensional ones, $\langle\ \rangle$ stands for the mean over the cross section of the duct and $d_h^*$ is the hydraulic diameter. The main axial velocity $\langle\omega^*\rangle$ is calculated by

$$\langle\omega^*\rangle = \frac{\nu}{4\sqrt{2\delta d}}\int_{-1}^{1} dx \int_{-1}^{1} \omega(x,y,t)dy \tag{9}$$

Since $\left(P_1^* - P_2^*\right)/\Delta_{z^*} = G$, $\lambda$ is related to the mean non-dimensional axial velocity $\langle\omega\rangle$ as

$$\lambda = \frac{32\sqrt{2\delta}\,Dn}{5\langle\omega\rangle^2} \tag{10}$$

where $\langle\omega\rangle = \sqrt{2\delta d}\langle\omega^*\rangle/\nu$. Equation (10) will be used to find the resistance coefficient of the flow evolution by numerical calculations.

## 5. Results and Discussion

### 5.2. Case I: Unsteady Solutions for $\delta = 0.001$

We first investigate time evolution of $\lambda$ for $Dn = 100$ and $Dn = 175$ as shown in Figs. 2(a) and 3(a) respectively. It is found that the unsteady flow is a steady-state solution for $Dn = 100$ and $Dn = 175$. To draw the contours of secondary flow ($\psi$) and axial flow ($w$), we use the increments $\Delta\psi = 0.6$ and $\Delta w = 0.8$, respectively. The same increments of $\psi$ and $w$ are used for all the figures in this paper, unless specified. The right-hand side of each duct box of $\psi$ and $w$ is in the outside direction of the duct curvature. In the figures of the streamlines, solid lines ($\psi \geq 0$) show that the secondary flow is in the counter clockwise direction while the dotted lines $(\psi < 0)$ in the clockwise direction. Typical contours of secondary flow patterns and axial flow distributions are shown in Figure 2(b) for $Dn = 100$ at time $t = 10$ and in Figure 3(b) for $Dn = 175$ at time $t = 6$, and it is found that both the unsteady solutions are symmetric two-vortex solutions. It is also found that axial flow distribution is consistence with the secondary vortices and the maximum axial flow is distributed through the centre of the duct.

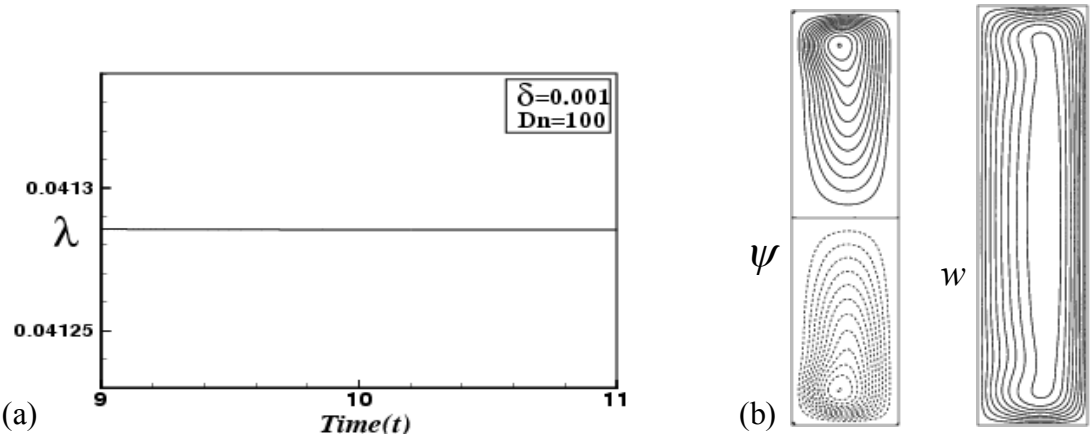


**Figure 2:** (a) Time evolution of λ for $Dn = 100$ and $\delta = 0.001$, (b) Secondary flow patterns (left) and axial flow distribution (right) for $Dn = 100$ at time $t = 10$.

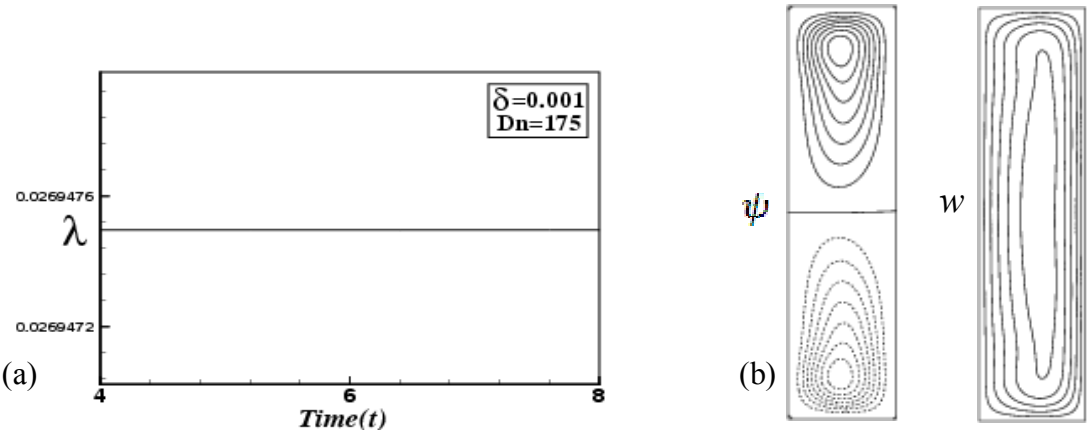


**Figure 3:** (a) Time evolution of λ for $Dn = 175$ and $\delta = 0.001$, (b) Secondary flow patterns (left) and axial flow distribution (right) for $Dn = 175$ at time $t = 6$.

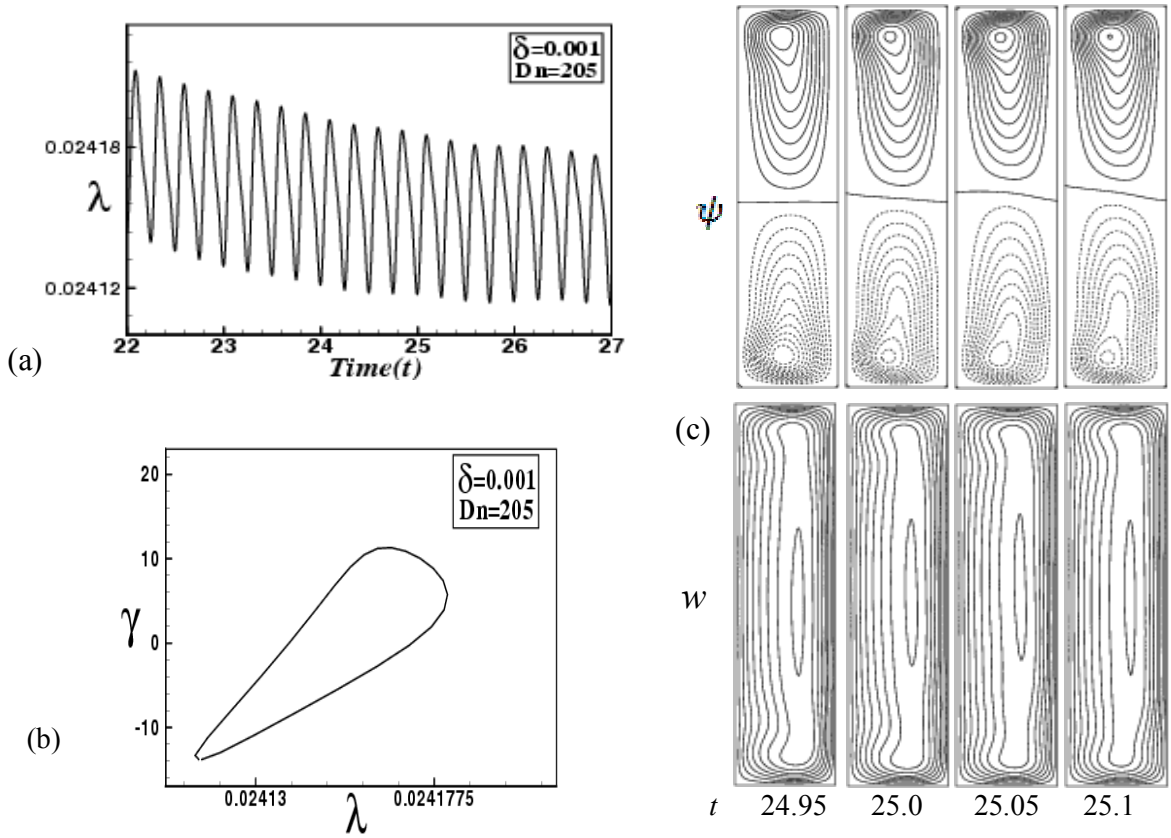


**Figure 4:** (a) Time evolution of λ for $Dn = 205$ and $\delta = 0.001$ (b) Phase space for $Dn = 205$, (c) Secondary flow patterns (top) and axial flow distribution (bottom) for $Dn = 205$

Time evolution of λ for $Dn = 205$ is then shown in Fig. 4(a). As seen in Fig. 4(a), the flow oscillates periodically for $Dn = 205$. The periodic solution is also well justified by drawing the phase space as shown in Fig. 4(b) in the $\lambda - \gamma$ plane, where $\gamma = \iint \psi \, dxdy$. As seen in Fig. 4(b), the flow creates a single orbit, which suggests that the flow is periodic. Typical contours of secondary flow patterns and axial flow distributions are then shown in Fig. 4(c), for one period of oscillation at time $24.95 \le t \le 25.10$, where it is seen that the unsteady flow at $Dn = 205$ oscillates between asymmetric two-vortex solutions. We also found that the axial flow distribution is consistent with the secondary flows and the axial flow is slightly shifted to the outer wall of the duct. Figure 5(a) shows time evolution result for $Dn = 210$, where we see that the unsteady flow is multi-periodic, which is well justified by drawing the phase space as shown in Fig. 5(b). In Fig. 5(b), we observe that the flow creates multiple orbits in its way, which suggests that the flow is multi-periodic at $Dn = 210$. Typical **c**ontours of secondary flow patterns and axial flow distribution, for one period of oscillation at time $22.30 \le t \le 22.52$, is shown in Fig. 5(c), where we observe that the flow oscillates between asymmetric two-vortex solutions. We also find that the axial flow distribution is consistent with the secondary vortices and the axial flow is shifted to the outer wall of the duct. It is found that the transition from periodic to multi-periodic oscillation occurs between $Dn = 205$ and $Dn = 210$.

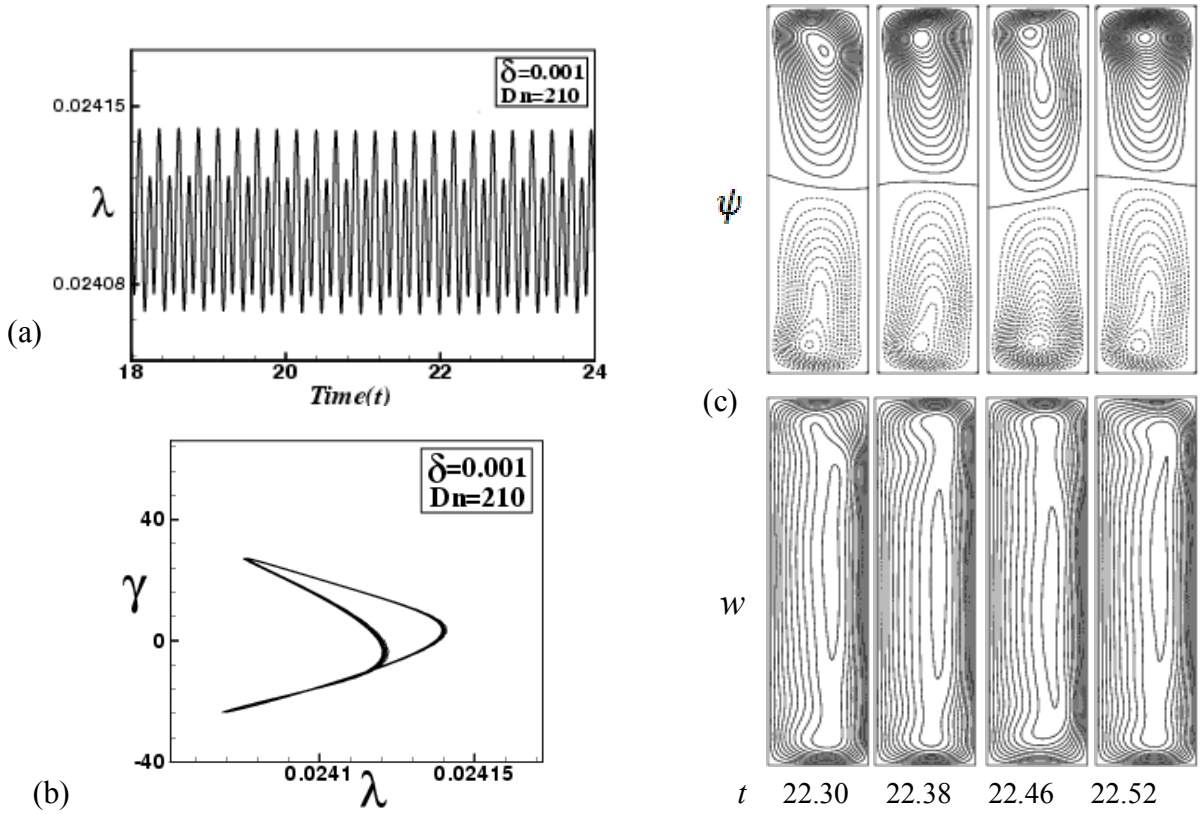


**Figure 5:** (a) Time evolution of λ for $Dn = 210$ and $\delta = 0.001$ (b) Phase space for $Dn = 210$, (c) Secondary flow patterns (top) and axial flow distribution (bottom) for $Dn = 210$

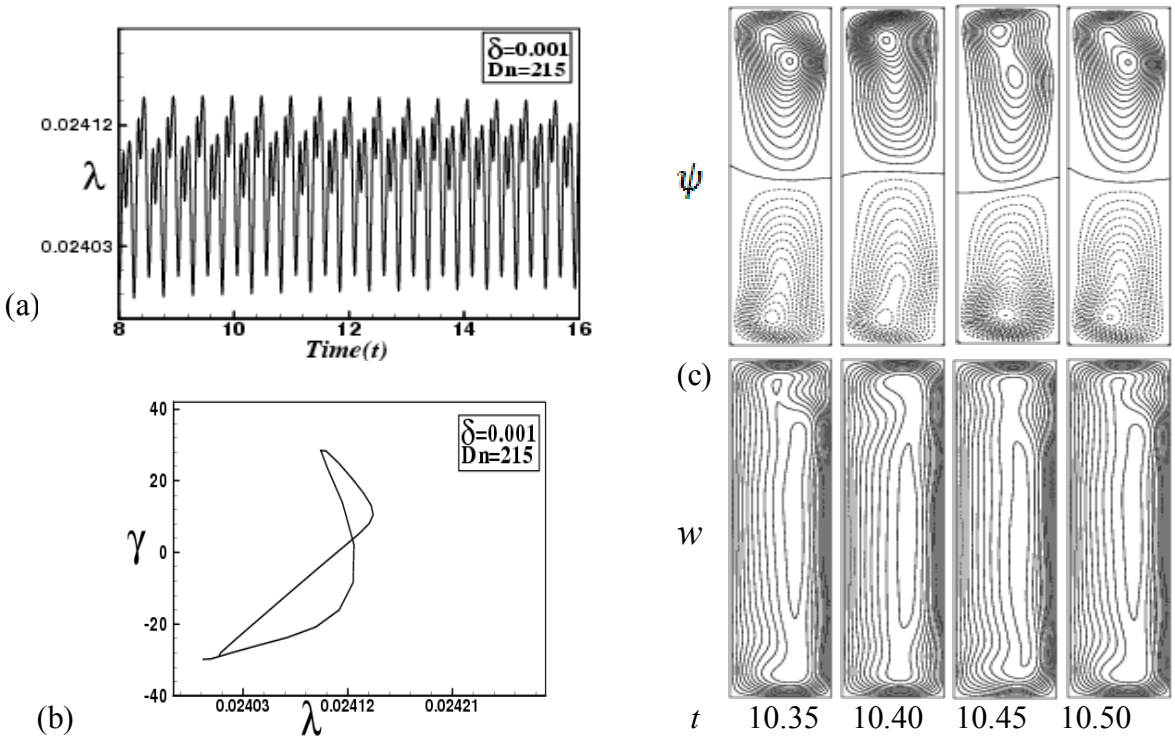


**Figure 6:** (a) Time evolution of λ for $Dn = 215$ and $\delta = 0.001$, (b) Phase space for $Dn = 215$, (c) Secondary flow patterns (top) and axial flow distribution (bottom) for $Dn = 215$.

The result of the time-dependent solution for $Dn = 215$ is shown in Fig. 6(a). We found that the flow is multi-periodic for $Dn = 215$, which is well justified by drawing the phase space as shown in Fig. 6(b). In Fig. 6(b), we observe that the flow creates a couple of orbit, which suggests that the flow is multi-periodic at $Dn = 215$. Contours of secondary flow patterns and axial flow distribution, for one period of oscillation at time $10.35 \le t \le 10.52$, are shown in Fig. 6(c), where we observe that the flow oscillates between asymmetric two-vortex solutions. By the time evolution calculation for $Dn = 220$, we find that the unsteady flow oscillates irregularly that means the flow is chaotic. Figure 7(a) shows the time evaluation result for $Dn = 220$. As seen in Figure 7(a) the time-dependent flow oscillates irregularly so that the flow is chaotic. The chaotic oscillation is well justified by drawing the phase spaces as shown in Fig. 7(b). Figures 7(b) shows that there occurs irregular orbits, which signifies that the unsteady flow presented in Fig. 7(a) is chaotic. Then typical contours of secondary flow patterns and axial flow distribution for the chaotic oscillation at $Dn = 220$ are obtained as shown in Figure 7(c), where it is found that the unsteady solution for $Dn = 220$ makes asymmetric four-vortex solutions. We also found that the axial flow distribution is consistent with the secondary vortices and the axial flow shifted near the outer wall as time proceeds. Thus, it is found that the transition from multi-periodic to chaotic oscillation occurs between $Dn = 215$ and $Dn = 220$. We perform time evolution calculation of $\lambda$ for $Dn = 500$. Figure 8(a) shows the time evaluation results for $Dn = 500$ and $\delta = 0.001$. As seen in Figure 8(a), the time-dependent flow oscillates irregularly that means the flow is chaotic. The chaotic oscillation for $Dn = 500$ is well justified by drawing the phase spaces as shown in Fig. 8(b). Then typical contours of secondary flow patterns and axial flow distribution for $Dn = 500$ are shown in Fig. 8(c) for $11.4 \le t \le 11.7$, and it is found that the unsteady solution oscillates irregularly making asymmetric six- to eight-vortex solutions. We also found that the axial flow is shifted to the outer wall of the duct as time passes.

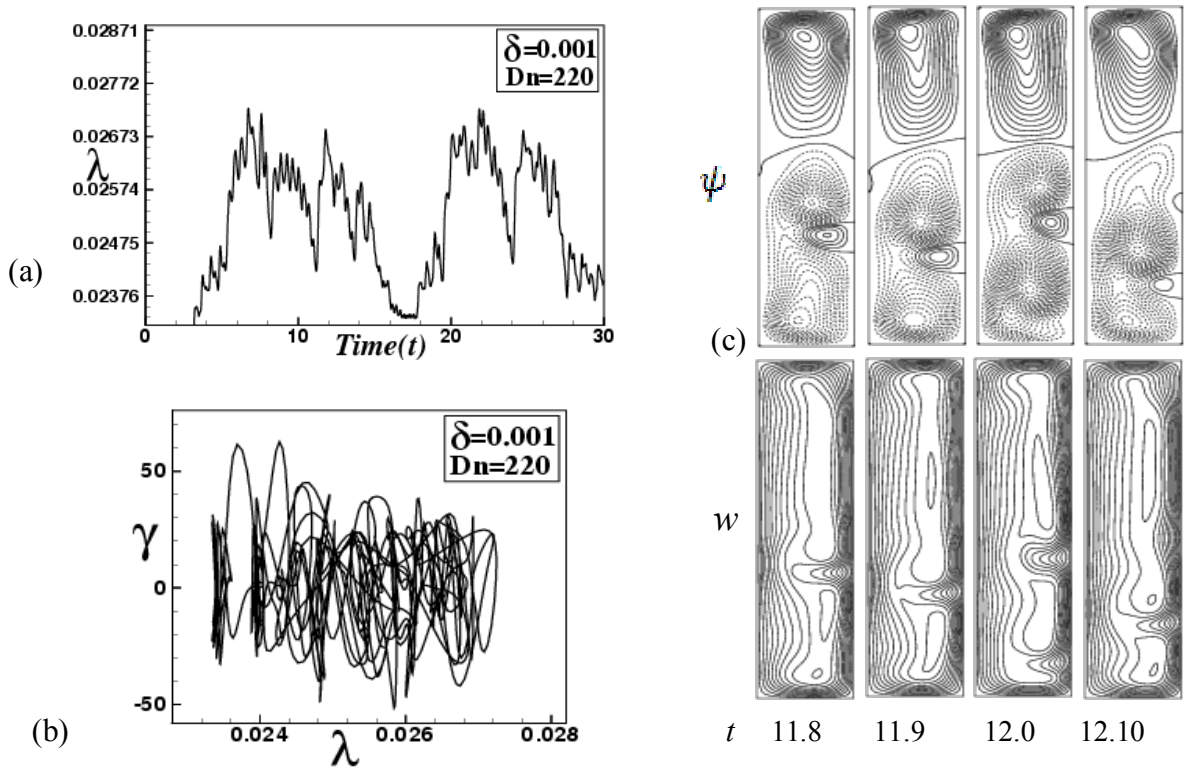


**Figure 7:** (a) Time evolution of λ for $Dn = 220$ and $\delta = 0.001$ (b) Phase space for $Dn = 220$, (c) Secondary flow patterns (top) and axial flow distribution (bottom) for $Dn = 220$.

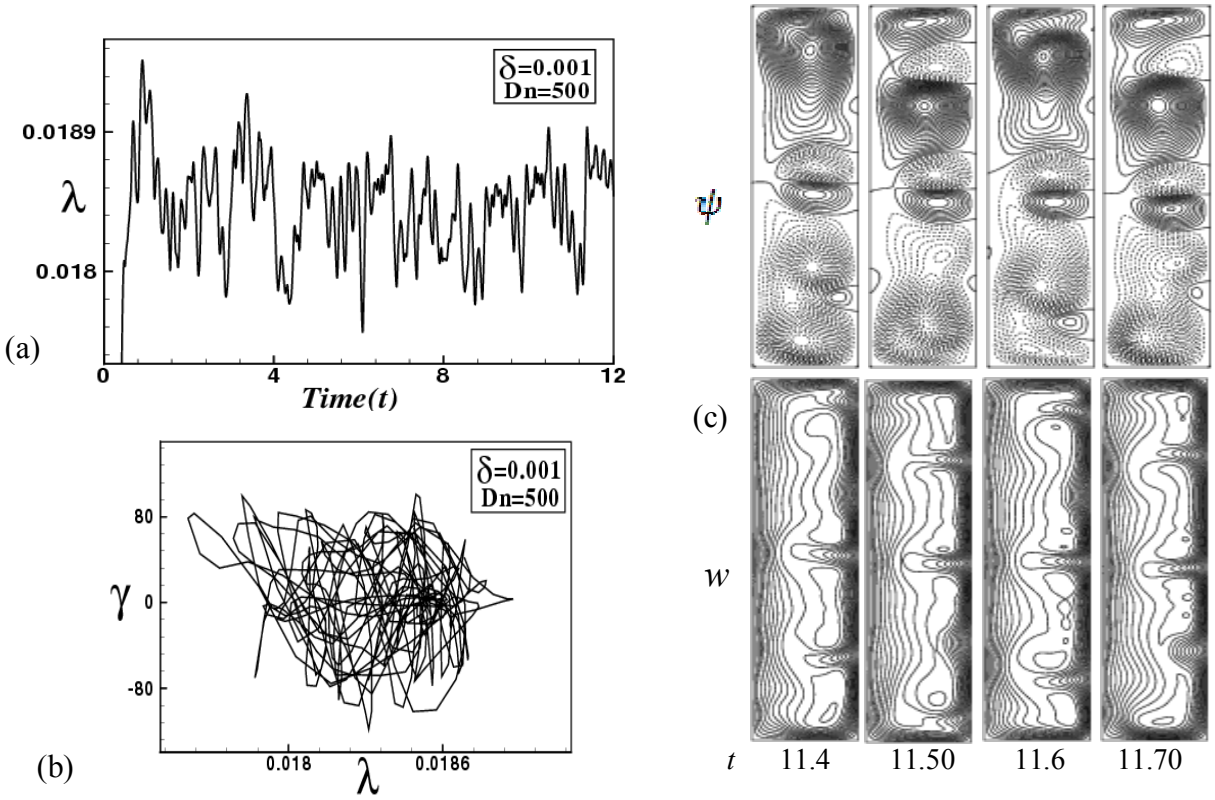


**Figure 8:** (a) Time evolution of $\lambda$ for $Dn = 500$ and $\delta = 0.001$ (b) Phase space for $Dn = 500$, (c) Secondary flow patterns (top) and axial flow distribution (bottom) for $Dn = 500$

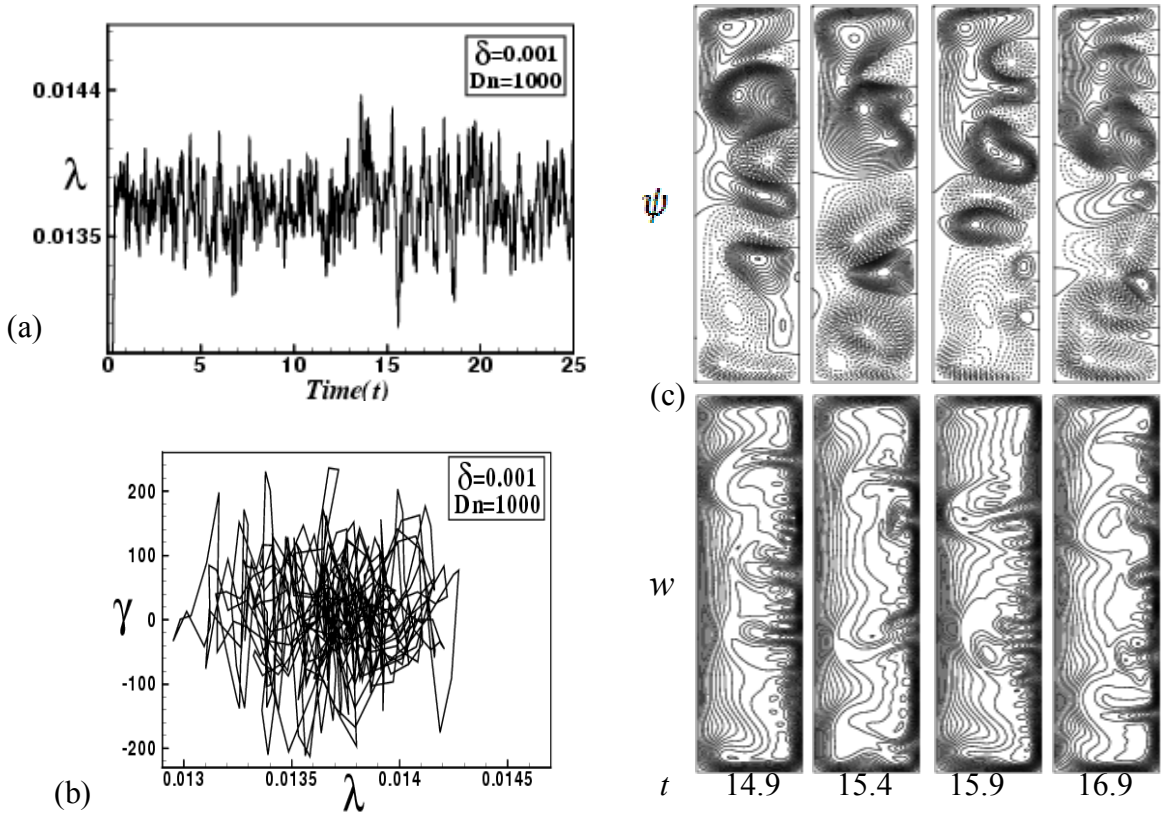


**Figure 9:** (a) Time evolution of $\lambda$ for $Dn = 1000$ and $\delta = 0.001$ (b) Phase space for $Dn = 1000$, (c) Secondary flow patterns (top) and axial flow distribution (bottom) for $Dn = 1000$

Then we studied time evolution calculation for $Dn = 1000$ as shown in Fig. 9(a). Figure 9(a) shows that the flow oscillates in strongly irregular pattern, i.e. the flow is *strong chaotic* for $Dn = 1000$. To justify the chaotic oscillation, we draw the phase space for $Dn = 1000$ as shown in Fig. 9(b), where multiple orbits are seen to be distributed irregularly, which suggests that the flow presented in Fig. 9(a) is strong chaotic (for details, see Mondal et al. [25]). To observe the change in the unsteady flow characteristics for $Dn = 1000$, typical contours of secondary flow patterns and axial flow distribution are shown in Fig. 9(c) at time $14.9 \le t \le 16.9$, where it is seen that the chaotic solution at $Dn = 1000$ oscillates between asymmetric eight- to twelve-vortex solutions. Here we see that the time dependent solutions are more chaotic than the previous solutions. We call this type of solution is *strong chaotic* (Mondal *et al.* [25]). We also found that the axial flow distribution is consistent with the secondary flows and the axial flow shifted to the outer wall of the duct as time proceeds.

### 5.2. Case II : Unsteady solutions for $\delta = 0.1$

In this sub-section, we investigated unsteady solutions of the flow through a curved rectangular duct of aspect ratio 4 and curvature $\delta = 0.1$. To obtain the unsteady solutions, we studied time evolution of the resistance coefficient $\lambda$. Figure 10(a) shows unsteady flow results for $Dn = 100$. As seen in Fig. 10(a), the unsteady flow is a steady-state solution for $Dn = 100$. Since the flow is steady-state, a single contour of the secondary flow pattern and axial flow distribution for $Dn = 100$ is shown in Fig. 10(b) at time $t = 8$, and it is found that the unsteady flow for $Dn = 100$ is a symmetric two-vortex solution.

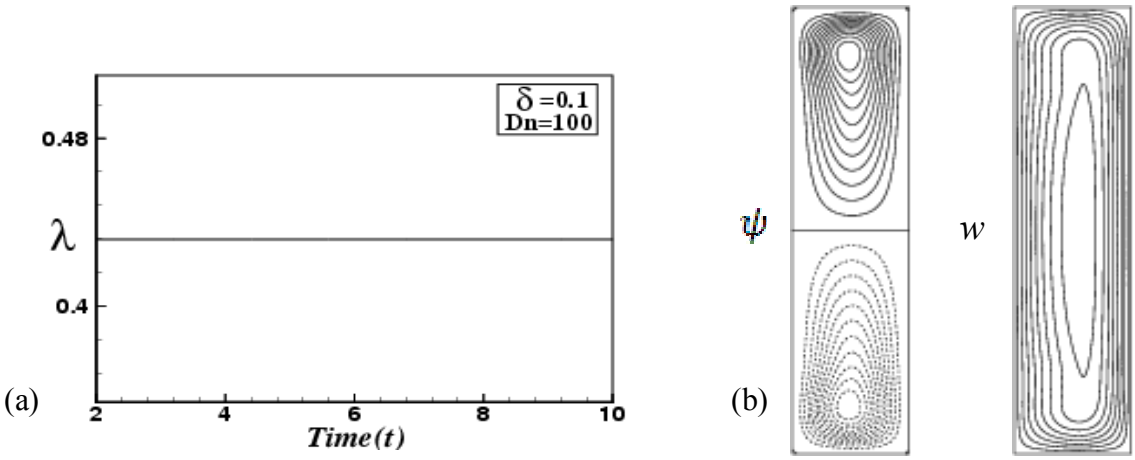


**Figure 10:** (a) Time evolution of $\lambda$ for $Dn = 100$ and $\delta = 0.1$ (b) Secondary flow patterns (left) and axial flow distribution (right) for $Dn = 100$ at time $t = 8$.

We then investigated time-dependent solution for $Dn = 230$ as shown in Fig. 11(a). It is found that the flow is a periodic oscillating for $Dn = 230$. The periodic solution is also well justified by drawing the phase space as shown in Fig. 11(b) in the $\lambda - \gamma$ plane, where $\gamma = \iint \psi \, dxdy$. As seen in Fig. 11(b), the flow creates a single orbit, which suggests that the flow is periodic. Typical contours of secondary flow patterns and axial flow distributions for the periodic oscillation, as time proceeds, are then obtained for $Dn = 230$ as shown in Figure 11(c), for one period of oscillation at time $13.0 \le t \le 13.20$, where it is seen that the unsteady flow at $Dn = 230$ oscillates between asymmetric two-vortex solutions. We also found that the axial flow distribution is consistent with the secondary flows and the axial flow is slightly shifted to the outer wall of the duct. By the time evolution calculation we obtained unsteady solutions for $Dn = 250$ as shown in Figure 12(a). It is

found that the flow oscillates irregularly but it can not be well determined. Then we draw phase space of the time-evolution result as shown in Fig. 12(b), and it is found that the flow oscillates irregularly with multiple orbits, which suggests that the flow presented in Fig. 12(a) is chaotic. This type of chaotic oscillation is termed as *weak chaos* (Mondal *et al*. [25]). Then typical contours of secondary flow patterns and axial flow distribution are shown in Figure 12(c) for $10.2 \le t \le 10.8$ and it is found that the unsteady solution oscillates between asymmetric two-, four- and five-vortex solutions. We also found that the axial flow distribution is consistent with the secondary flow and the axial flow shifted to the outer wall as time proceeds. It is found that the transition from periodic to chaotic oscillation occurs between $Dn = 230$ and $Dn = 250$ for $\delta = 0.1$.

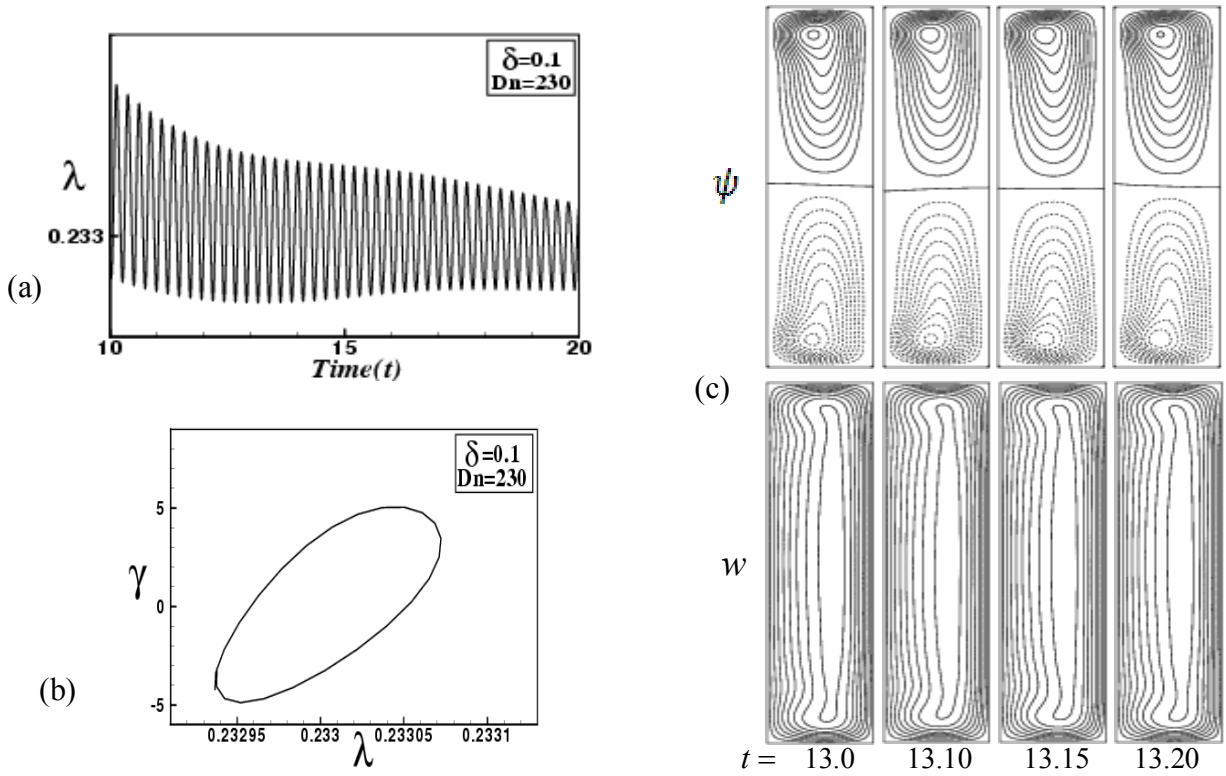


**Figure 11:** (a) Time evolution of λ for $Dn = 230$ and $\delta = 0.1$ (b) Phase space for $Dn = 230$ (c) Secondary flow patterns and axial flow distribution for $Dn = 230$

Then we perform the time evolution of $\lambda$ for $Dn = 300$. Figure 13(a) shows the time evaluation results for $Dn = 300$. As seen in Figure 13(a), the time-dependent flow oscillates irregularly so that the flow is chaotic. The chaotic oscillation is well justified by drawing the phase space as shown in Fig. 13(b). Figure 13(b) shows that the flow oscillates irregularly in a nonlinear pattern creating multiple orbits, which suggests that the flow is chaotic. Typical contours of secondary flow patterns and axial flow distributions are shown in Figure 13(c), for one period of oscillation at time $20.5 \le t \le 22.0$, and it is found that the chaotic flow is asymmetric four-, five- and six-vortex solutions. We also found that the axial flow distribution is consistent with the secondary vortices and the axial flow shifted near the outer wall of the duct. Next, we investigated time evolution of $\lambda$ for $Dn = 380$. Figure 14(a) shows time evaluation results for $Dn = 380$. As seen in Figure 14(a), the time-dependent solution oscillates irregularly which means the flow is chaotic, which is well justified by drawing a phase space of the time evolution result as shown in Fig. 14(b). Typical contours of secondary flow patterns and axial flow distributions are shown in Figure 14(c) for time interval $10.2 \le t \le 10.8$ and it is found that the unsteady flow for $Dn = 380$ makes asymmetric four- and five-vortex solutions.

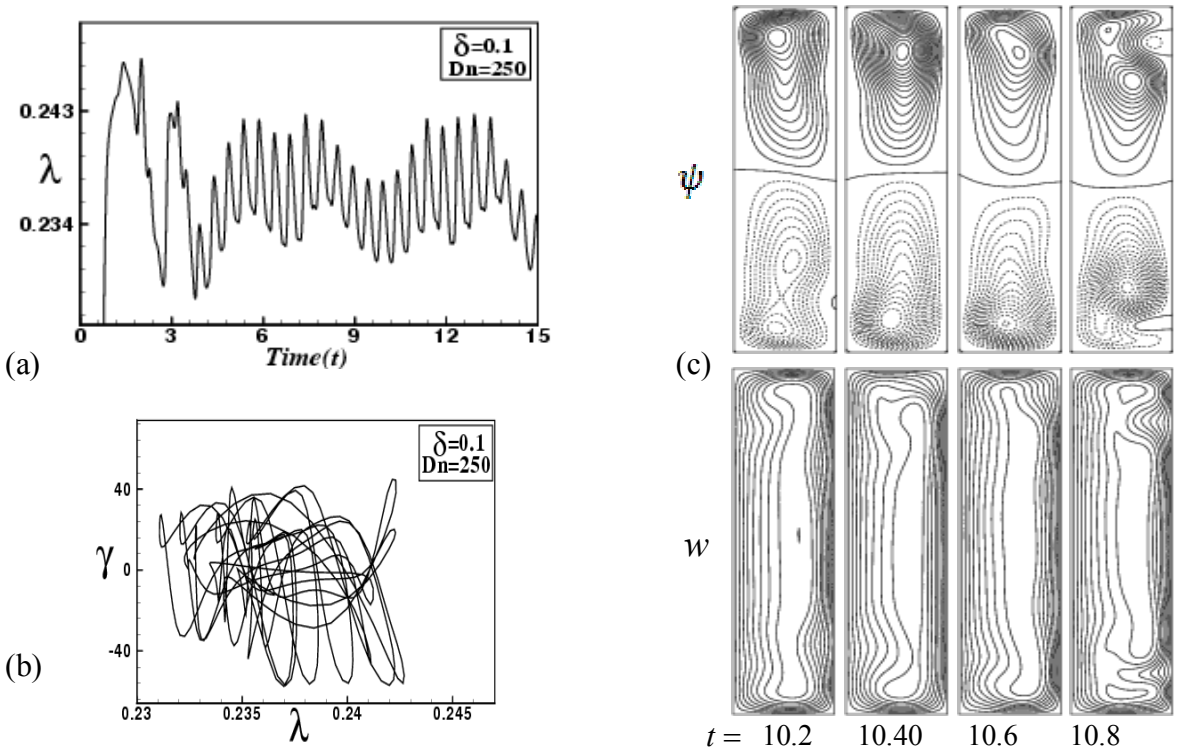


**Figure 12:** (a) Time evolution of λ for $Dn = 250$ and $\delta = 0.1$ (b) Phase space for $Dn = 250$ (c) Secondary flow patterns and axial flow distribution for $Dn = 250$

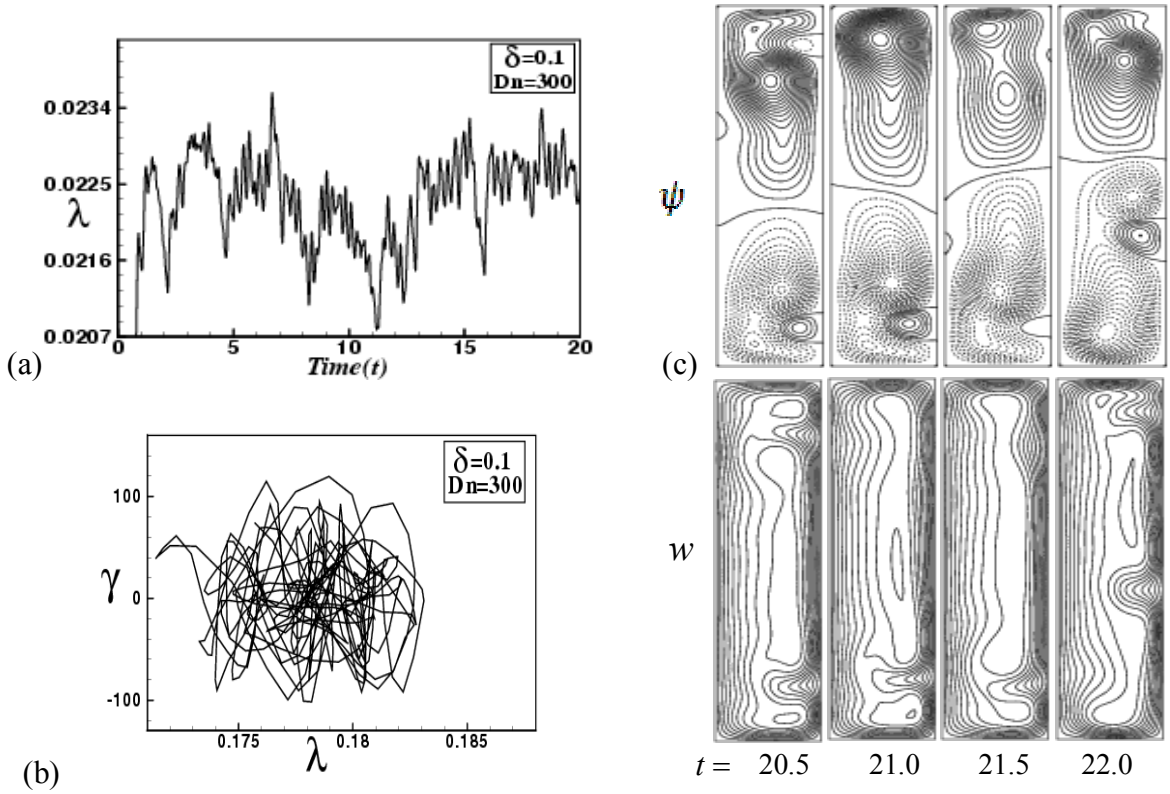


**Figure 13:** (a) Time evolution of λ for $Dn = 300$ and $\delta = 0.1$ (b) Phase space for $Dn = 300$, (c) Secondary flow patterns (top) and axial flow distribution (bottom) for $Dn = 300$.

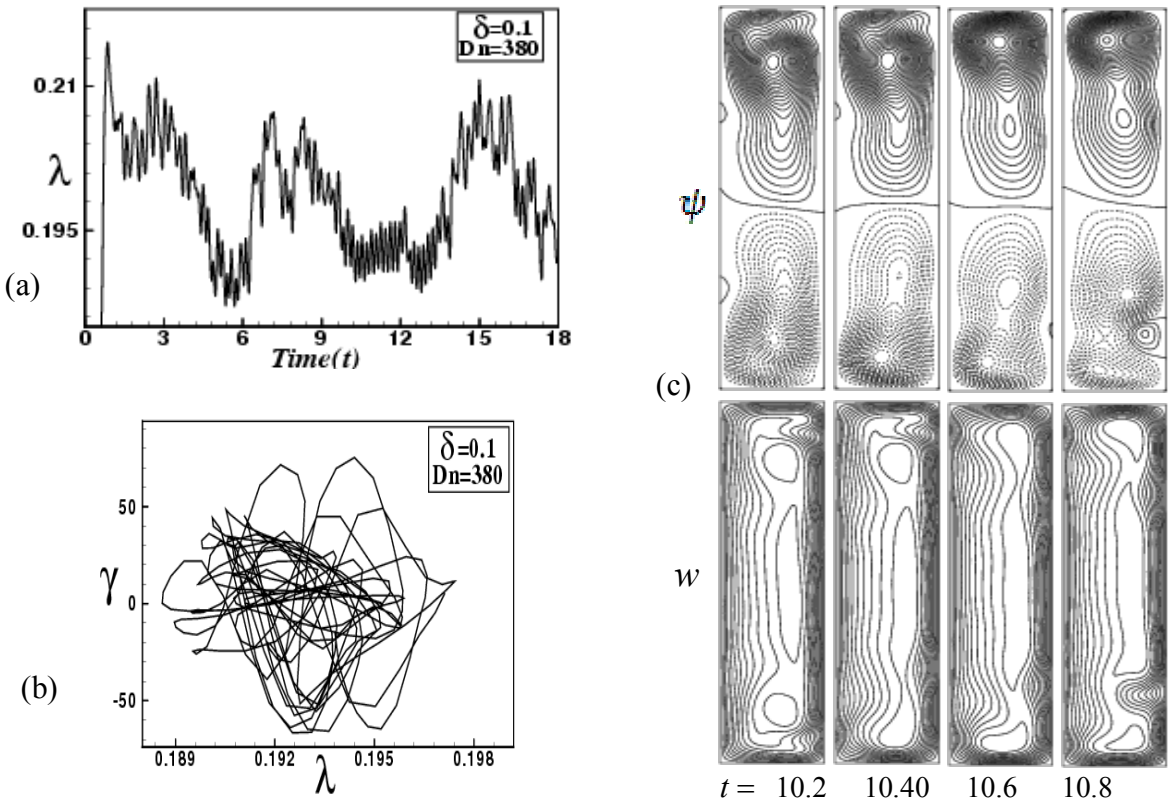


**Figure 14:** (a) Time evolution of λ for $Dn = 380$ and $\delta = 0.1$, (b) Phase space for $Dn = 380$, (c) Secondary flow patterns (top) and axial flow distribution (bottom) for $Dn = 380$.

We studied time-dependent solution of λ for $Dn = 390$ as shown in Fig. 15(a). It is found that the flow is oscillates periodically for $Dn = 390$. However, to justify whether the flow is periodic or multi-periodic, we sketch phase space of the time evolution result as shown in Fig. 15(b). Figure 15(b) shows that the unsteady flow at $Dn = 390$ creates multiple orbits so that the flow is multi-periodic rather than periodic. With a view to observe the change in secondary flow characteristics of the multi-periodic oscillation, as time proceeds, typical contours of secondary flow patterns and axial flow distributions are shown in Fig. 15(c), for one period of oscillation at time $10.3 \le t \le 10.45$, and it is seen that the flow oscillates between asymmetric five- and six-vortex solutions. We also found that the axial flow distribution is consistent with the secondary vortices and the axial flow is shifted to the outer wall as $Dn$ becomes large. Figure 16(a) shows time evolution result for $Dn = 400$, where we see that the unsteady flow is also multi-periodic which is well justified by drawing the phase space as shown in Fig. 16(b). In Fig. 16(b), we observe that the flow creates multiple orbits, which suggests that the flow is multi-periodic at $Dn = 400$. Contours of secondary flow patterns and axial flow distributions is then shown in Figure 16(c) for $Dn = 400$, for one period of oscillation at time $42.2 \le t \le 42.35$, where it is seen that the flow at $Dn = 400$ oscillates between asymmetric four- and six-vortex solutions. We also found that the axial flow distribution is consistent to the secondary flow and the axial flow is slightly shifted to the outer wall of the duct.

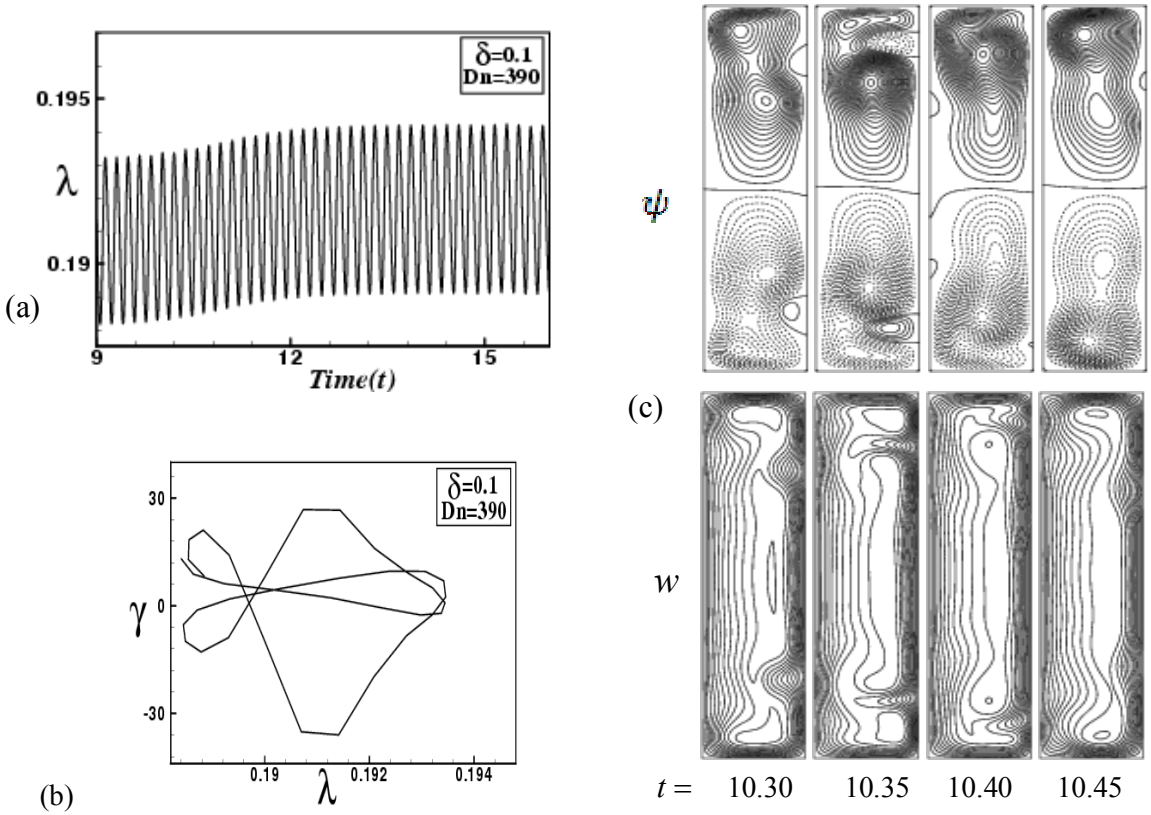


**Figure 15:** (a) Time evolution of λ for $Dn = 390$ and $\delta = 0.1$, (b) Phase space for $Dn = 390$, (c) Secondary flow patterns (top) and axial flow distribution (bottom) for $Dn = 390$

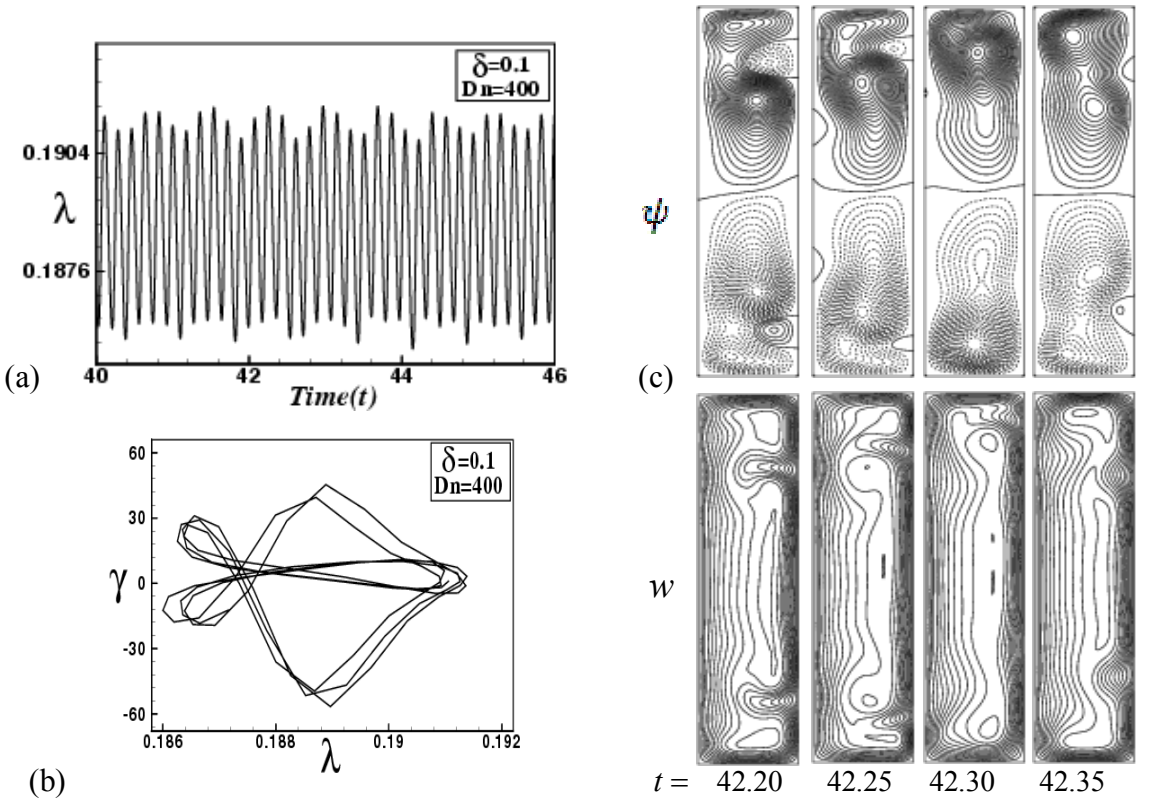


**Figure 16:** (a) Time evolution of λ for $Dn = 400$ and $\delta = 0.1$ (b) Phase space for $Dn = 400$, (c) Secondary flow patterns (top) and axial flow distribution (bottom) for $Dn = 400$.

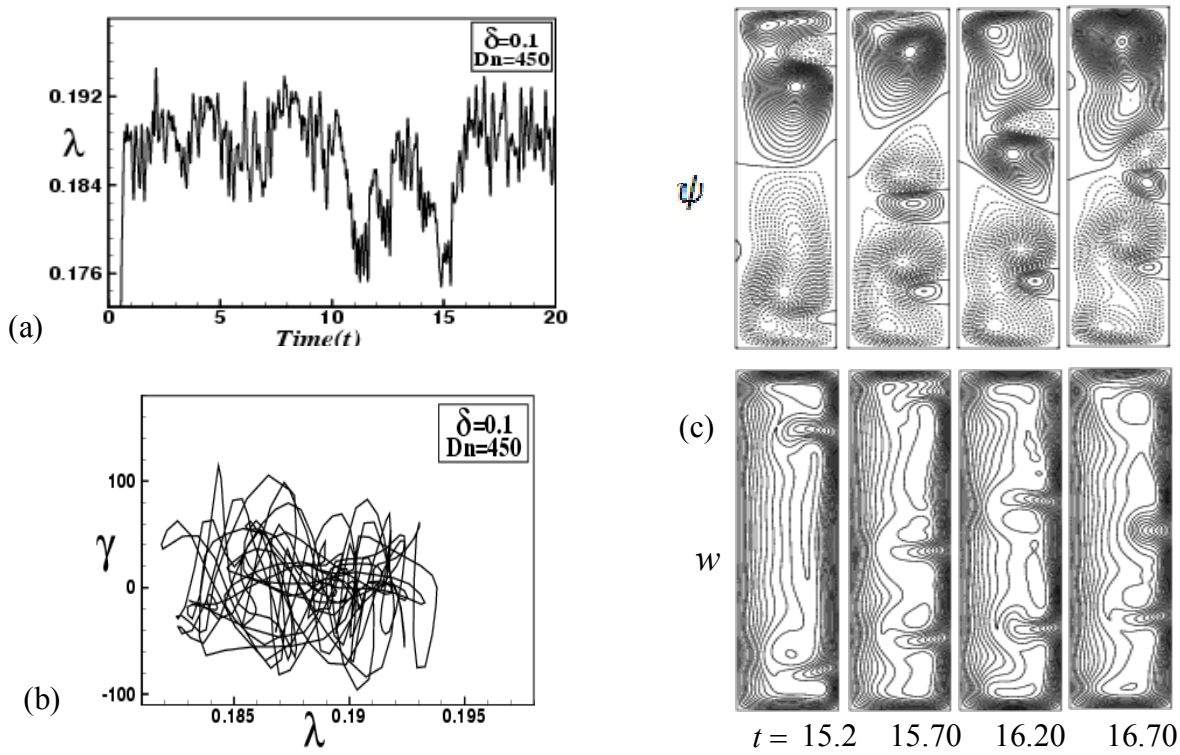


**Figure 17:** (a) Time evolution of λ for $Dn = 450$ and $\delta = 0.1$, (b) Phase space for $Dn = 450$, (c) Secondary flow patterns (top) and axial flow distribution (bottom) for $Dn = 450$

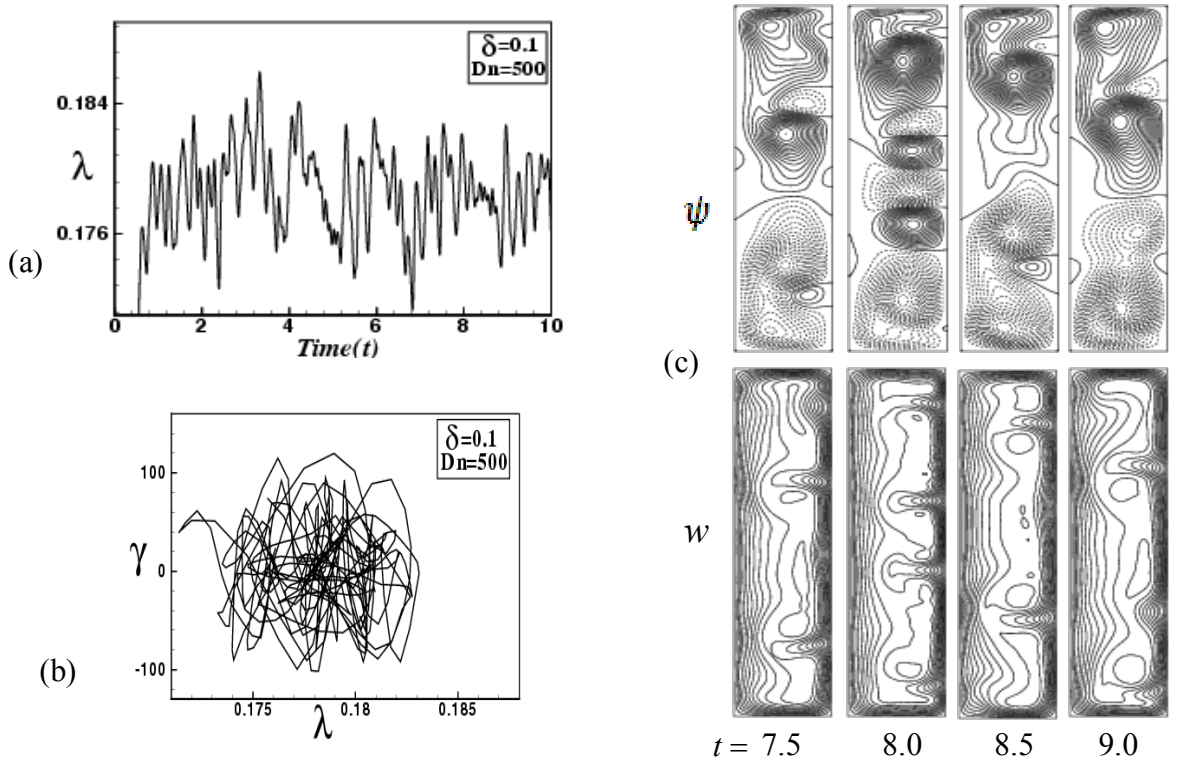


**Figure 18:** (a) Time evolution of λ for $Dn = 500$ and $\delta = 0.1$, (b) Phase space for $Dn = 500$, (c) Secondary flow patterns (top) and axial flow distribution (bottom) for $Dn = 500$

We perform time evolution of $\lambda$ for $Dn = 450$ and $\delta = 0.1$. Figure 17(a) shows time evaluation results for $Dn = 450$. As seen in Figure 17(a), the time-dependent flow oscillates irregularly in a non-linear pattern so that the flow is chaotic. The phase space of the chaotic oscillation is shown in Fig. 17(b), where we clearly observe the chaotic orbits of the line spectrum. Typical contours of secondary flow patterns and axial flow distributions are then shown in Fig. 17(c) for time $15.2 \le t \le 17.2$ and it is found that the unsteady flow is an asymmetric five- and six-vortex solutions. We also found that the axial flow distribution is consistent with the secondary flows and the axial flow shifted to the outer wall. In this study, it is found that the transition from multi-periodic to chaotic oscillation occurs between $Dn = 400$ and $Dn = 450$. Then we performed time evolution of $\lambda$ for $Dn = 500$ and $\delta = 0.1$ as shown in Figure 18(a). As seen in Figure 18(a), the time-dependent flow oscillates irregularly so that the flow is chaotic. To observe the characteristics of the chaotic oscillation, a phase space of the chaotic flow for $Dn$ = 500 is shown in Fig. 18(b). Typical contours of secondary flow patterns and axial flow distributions are shown in Figure 18(c) for $7.5 \le t \le 9.0$ and it is found that the chaotic flow oscillates between asymmetric seven- and eight-vortex solutions.

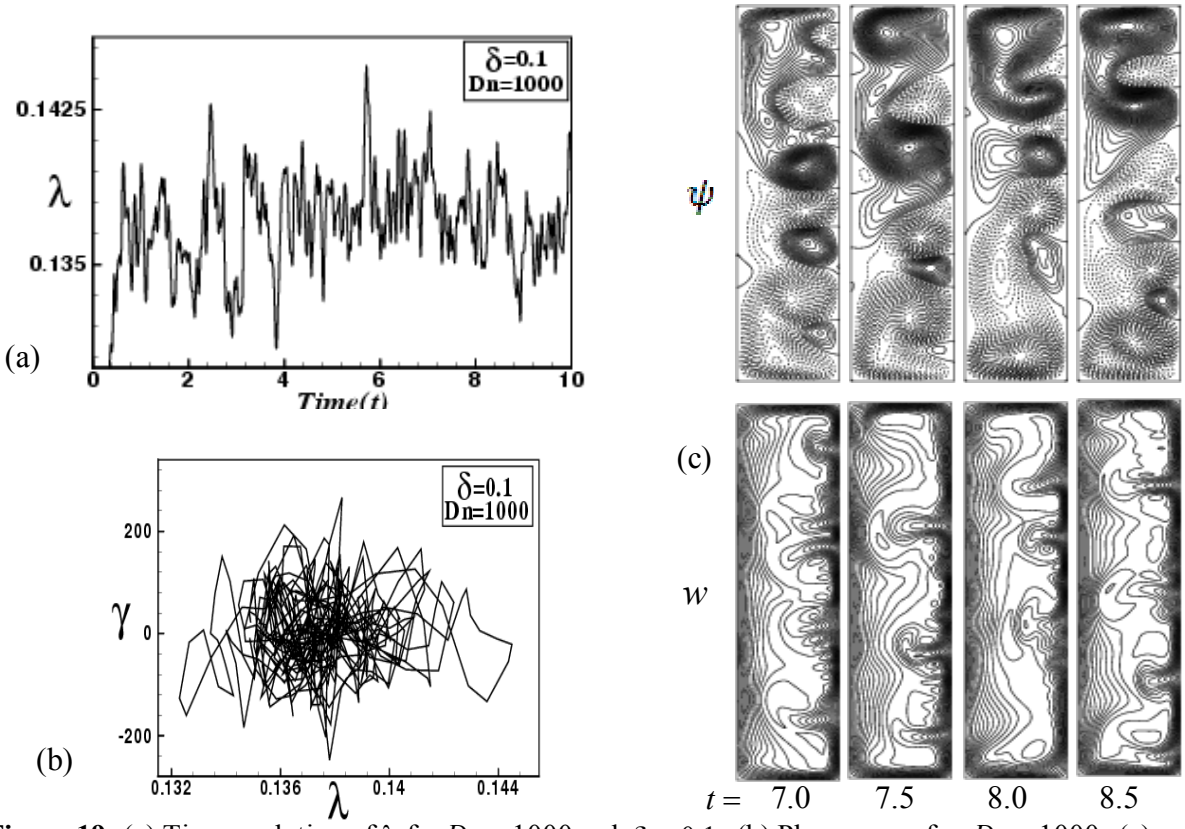


**Figure 19:** (a) Time evolution of λ for $Dn = 1000$ and $\delta = 0.1$, (b) Phase space for $Dn = 1000$, (c) Secondary flow patterns (top) and axial flow distribution (bottom) for $Dn = 1000$

Then we studied the time evolution of $\lambda$ for $Dn = 1000$ as shown in Fig. 19(a). We find that the flow is strong chaotic for $Dn = 1000$. To observe the change in the flow characteristics, contours of secondary flow patterns and axial flow distribution are shown in Fig. 19(b), where it is seen that the chaotic solution at $Dn = 1000$ oscillates between asymmetric eight-, nine- and ten-vortex solutions. We found that the axial flow distribution is consistence with the secondary vortices and the axial flow is shifted near the outer wall as $Dn$ increases. In fact, the periodic oscillation, which is observed in the present study, is a traveling wave solution advancing in the downstream direction which is well justified in the recent investigation by Yanase *et al*. [29] for a three-dimensional (3D) travelling wave solutions as an appearance of 2D periodic oscillation.

## 6. Conclusions

In this paper, a comprehensive numerical study is presented for the unsteady solutions of flow through a curved rectangular duct of aspect 4 by using a spectral method, and covering a wide range of the Dean number for two types of duct curvatures, $\delta = 0.001$ and $\delta = 0.1$.

At first, we investigated unsteady solutions for the small curvature $\delta = 0.001$. It is found that the unsteady flow is a steady-state solution for $Dn = 100$ and $Dn = 175$, which creates symmetrical two vortices. It is found that the flow is periodic for $Dn = 205$ but multi-periodic for $Dn = 210$ and $Dn = 215$. Secondary flow patterns show that the periodic flow oscillates asymmetrically between two-vortex solutions while multi-periodic flows between asymmetric two- and three-vortex solutions. If $Dn$ is increased further, the flow becomes chaotic and remains chaotic up to $Dn = 1000$. It is also found that the unsteady flow is a *weak chaos* for $Dn = 220$ but *strong chaos* for $Dn = 500$ and at larger $Dn$'s. Typical contours of secondary flow patterns and axial flow distribution show that the flow oscillates periodically/multi-periodically between asymmetric four-, six- and eight-vortex solutions, while chaotic flows between asymmetric eight- to twelve-vortex solutions, and the unsteady flow for $\delta = 0.001$ undergoes in the scenario '*steady-state* $\rightarrow$ *periodic* $\rightarrow$ *multi-periodic* $\rightarrow$ *weak chaotic* $\rightarrow$ *strong chaotic'*, if $Dn$ is increased. Then we studied unsteady solutions for the moderate curvature $\delta = 0.1$, and it is found that the unsteady flow is a steady-state solution for $Dn = 100$ but periodic for $Dn = 230$. The steady-state or periodic flow consists of symmetric two-vortex solutions. It is found that the unsteady flow is chaotic solution for $Dn = 250$ to $Dn = 380$, and this chaotic flow oscillates irregularly between asymmetric two-, four-, five- and six-vortex solutions. Unsteady solutions for large $Dn$`s show that the flow is always chaotic, which oscillates asymmetrically between four- to ten-vortex solutions, and the unsteady flow for $\delta = 0.1$ undergoes through various flow instabilities in the scenario '*steady-state* $\rightarrow$ *periodic* $\rightarrow$ *chaotic* $\rightarrow$ *periodic* $\rightarrow$ *multi-periodic* $\rightarrow$ *chaotic*', if $Dn$ is increased. Phase spaces were found to be very fruitful to identify the transitional process from periodic to multi-periodic and multi-periodic to chaotic oscillation very clearly. In this regard, it should be worth mentioning that irregular oscillation of the isothermal flow through a curved rectangular duct has been observed experimentally by Ligrani and Niver [6] for the large aspect ratio.

## References

[1] Dean, W. R., Note on the motion of fluid in a curved pipe, *Philos. Mag*., 4, 208–223, 1927.
[2] Berger, S.A., Talbot, L. and Yao, L. S., Flow in Curved Pipes, *Annual. Rev. Fluid. Mech*., 35, pp. 461-512, 1983.
[3] Nandakumar, K. and Masliyah, J. H., Swirling Flow and Heat Transfer in Coiled and Twisted Pipes, *Adv. Transport Process*., 4, pp. 49-112, 1986.
[4] Ito, H, Flow in Curved Pipes, *JSME Int. J*., 30, pp. 543-5, 1987.
[5] Akiyama, M., Kikuchi, K., Nakayama, J., Nishiwaki, I. and Cheng, K. C., Hydraulically unstable flow, interactions of the boundary type secondary flows and their steplike development of transition, *Trans. JSME*, Ser. B47, 1705, 1981.
[6] Ligrani, P. M. and Niver, R. D., Flow visualization of Dean vortices in a curved channel with 40 to 1 aspect ratio, *Phys. Fluids*, 31, 3605, 1988.
[7] Yamamoto, K., Wu, X., Nozaki, K. and Hayamizu, Y., Visualization of Taylor–Dean flow in a curved duct of square cross-section, *Fluid Dyn. Res*., 38(1), 1-18, 2006.
[8] Bara, B. M., Experimental investigation of developing and fully developed flow in a curved duct of square cross section, *Ph.D. dissertation*, University of Alberta, 1991.
[9] Bara, B. M., Nandakumar, K. and Masliyah, J. H., An experimental and numerical study of the Dean problem: flow development towards two dimensional multiple solutions, *J. Fluid Mech*. 244, 339, 1992.

[10] Baylis, J. A., Experiments on laminar flow in curved channels of square section, *Journal of Fluid Mechanics*, 48(3), 417-422, 1971.
[11] Humphrey, J. A. C., Taylor, A. M .K., Whitelaw, Laminar flow in a square duct of strong curvature, *Journal of Fluid Mechanics,* 83, 509-527, 1977.
[12] Cheng, K. C., Nakayama, J. and Akiyama, M., Effect of Finite and Infinite Aspect Ratios on Flow Patterns in Curved Rectangular Channels, in: *Flow Visualization International Symposium*, Tokyo, 181, 1977.
[13] Ghia, K. N. and Sokhey, J. S., Laminar incompressible viscous flow in curved ducts of rectangular cross-section, *Trans, ASME I: Journal of Fluids Engineering*, 99, 640-648, 1977.
[14] Sugiyama, T. Hayashi, T. and Yamazaki, K., Flow characteristics in the curved rectangular channels, *Bulletin of JSME*, 26(216), 532-552, 1983.
[15] Chandratilleke, T. T. and Nursubyakto, Numerical prediction of secondary flow and convective heat transfer in externally heated curved rectangular ducts, *Int. J. Thermal Sciences*, 42, Issue 2, 187-198, 2003.
[16] Yanase, S. Mondal, R. N. and Kaga, Y., Numerical Study of Non-isothermal Flow with Convective Heat Transfer in a Curved Rectangular Duct, *Int. J. Thermal Sciences*, 44, 1047-1060, 2005.
[17] Norouzi, M., Kayhani, M. H., Shu, C. and Nobari, M. R. H., Flow of second-order fluid in a curved duct with square cross-section, *Journal of Non-Newtonian Fluid Mechanics*, 165, 323–339, 2010.
[18] Chandratilleke, T. T., Nadim, N. and Narayanaswamy, R., Vortex structure-based analysis of laminar flow behaviour and thermal characteristics in curved ducts, *Int. J. Thermal Sciences*, 59, 75-86, 2012.
[19] Norouzi, M. and Biglari, N., An analytical solution for Dean flow in curved ducts with rectangular cross section, *Physics of Fluids*, 25, 053602, 1-15, 2013.
[20] Yanase, S. and Nishiyama, K., On the bifurcation of laminar flows through a curved rectangular tube, *J. Phys. Soc. Japan*, 57(11), 3790-3795, 1988.
[21] Yanase, S., Kaga, Y. and Daikai, R., Laminar flow through a curved rectangular duct over a wide range of the aspect ratio, *Fluid Dynamics Research*, 31, 151-183, 2002.
[22] Wang, L. and Liu, F., Forced convection in tightly coiled ducts: Bifurcation in a high Dean number region, *International Journal of Non-Linear Mechanics*, 42, 1018 – 1034, 2007.
[23] Yanase, S., Mondal, R. N., Kaga, Y. and Yamamto, K.,Transition from steady to Chaotic States of Isothermal and Non-isothermal Flows through a curved Rectangular Duct, *Journal of the Physics Society of Japan*, 74(1), 345-358, 2005.
[24] Mondal, R. N., Kaga, Y., Hyakutake, T. and Yanase, S., Effects of curvature and convective heat transfer in curved square duct flows, *Trans. ASME, Journal of Fluids engineering*, 128 (9), 1013—1023, 2006.
[25] Mondal, R. N., Kaga, Y., Hyakutake, T. and Yanase, S., Bifurcation diagram for two-dimensional steady flow and unsteady solutions in a curved square duct, *Fluid Dynamics Research*, 39, 413-446, 2007.
[26] Mondal, R. N., Islam, S., Uddin, K. and Hossain, M. A., Effects of aspect ratio on unsteady solutions through curved duct flow, *Applied Mathematics and Mechanics*, 34(9), 1107–1122, 2013.
[27] Gottlieb, D. and Orazag, S. A., Numerical Analysis of Spectral Methods*, Society for Industrial and Applied Mathematics*, Philadelphia, USA, 1977.
[28] Mondal, R. N., Isothermal and Non-isothermal flows through curved duct with square and rectangular cross-section, *Ph.D. Thesis,* Department of Mechanical Engineering, Okayama University, Japan, 2006.
[29] Yanase, S., Watanabe, T and Hyakutake. T., Traveling-wave solutions of the flow in a curved-square duct, *Physics of Fluids*, 20, 124101, 1-8, 2008.